On car steering torques at parking speeds

R. S. Sharp* and R. Granger[#]
*Electrical and Electronic Engineering, Imperial College of Science, Technology and Medicine, Exhibition Road, London SW7 2BT
[#]Jaguar Cars Ltd, Engineering Centre, Abbey Road, Coventry CV3 4LF

Abstract: The steering torque at the handwheel, necessary to steer a car at zero speed, is discussed. Measurements made on a tyre alone on a static rig and measurements made on a car in normal trim are complemented by a mathematical system model. The model uses parameter values deriving partly from the tyre rig results, partly from the car specification and partly from the car results. It provides simulated behaviour matching that from the car experiments. It therefore provides a basis for understanding the results obtained and for predicting the results of design and operating changes. The various physical mechanisms involved in the steering torque are identified and their relative magnitudes, for the case considered, are established. The role of steering offset receives particular attention.

Keywords: Car, steering, torque, parking, measurement, theory

NOTATION

A; lower point on king-pin – see Appendix A
C; left wheel centre – see Appendix A
F; steering rack friction force magnitude
G; steering ratio, hand wheel to road wheel – see Appendix A
M; limiting tyre friction moment magnitude
O; upper point on king-pin – see Appendix A
W_r; W_l; wheel loads – see Appendix A
d; perpendicular distance from wheel centre to steer axis – see Appendix A
p; tyre inflation pressure
p_0; special value of inflation pressure, equation (2)
r; radius for area element in contact patch
R; radius of (circular) tyre to ground contact patch
β; smoothing coefficient for friction force and moments
χ; king-pin inclination angle – see Appendix A
$\dot{d}_w$; road wheel steering velocity
ε; castor angle – see Appendix A
φ; angle for area element in contact patch
μ; coefficient of friction between tyre and road
τ; steer torque at handwheel – see Appendix A

1 INTRODUCTION

The steering hand wheel torque needed to move the road wheels slowly against various forms of resistance at very low or zero vehicle speed is an important case in the design of a car steering system. It influences the choice of steering gear ratio, whether or not power assistance is necessary and the nature of such power assistance, if any. The present increasing use of electrical assistance and new considerations of “steer by wire” systems make the subject topical, although there seems to be little recent relevant literature.

As pointed out by Gough [1], the torque required to steer the road wheels of a car is a maximum when the car is stationary, so this is the case considered. Gough also outlined a simple way of treating the tyre to ground interaction for this case. In addition to this interaction, the steering geometry and the friction forces in the system influence the torque necessary. Although it is commonly believed that the torque can be reduced by increasing the offset distance of the tyre contact centre from the king-pin axis as put forward by Taborek [2], Gough stated that this is not the case, suggesting that the reduction of tyre force by rolling of the tyre is countered by the increase in the moment arm of the force, consequent on the increased offset. Hard evidence on the matter is lacking. The research reported is aimed at providing such evidence and increasing understanding of the issues.

Measurements of torque and other variables have been made on a static tyre rig and on a stationary car in various conditions. Experimental arrangements are described and results are given. The tyre rig is covered in section 2, while the car measurements are the subject of section 3. A mathematical model of the car steering system is set up in section 4, which includes results from the model. The results are interpreted in section 5 and conclusions are drawn in section 6. A brief analysis of the lifting effect of steering, with its influences on steering torque, is given in Appendix A.

2 STATIC TYRE RIG MEASUREMENTS

The static tyre rig is shown diagrammatically in Fig. 1. It provides for the location of the test wheel with freedom to spin about a fixed horizontal axis, while load is applied to the contact patch through a loading plate, supported by an aerostatic bearing. Torques applied to the loading plate through a turnbuckle and cable system can be measured, as can the load on the tyre and, of course, the tyre inflation pressure. A circular pin can be used to define a vertical axis of rotation for the loading plate. In the standard condition, the axis of this pin passes through the centre of the loading plate, which is also the centre of the contact patch, as shown in Fig. 2. Moving the pin in the y-direction simulates the inclusion of offset in a car steering system. The spin angle of the wheel can be measured with an inclinometer.

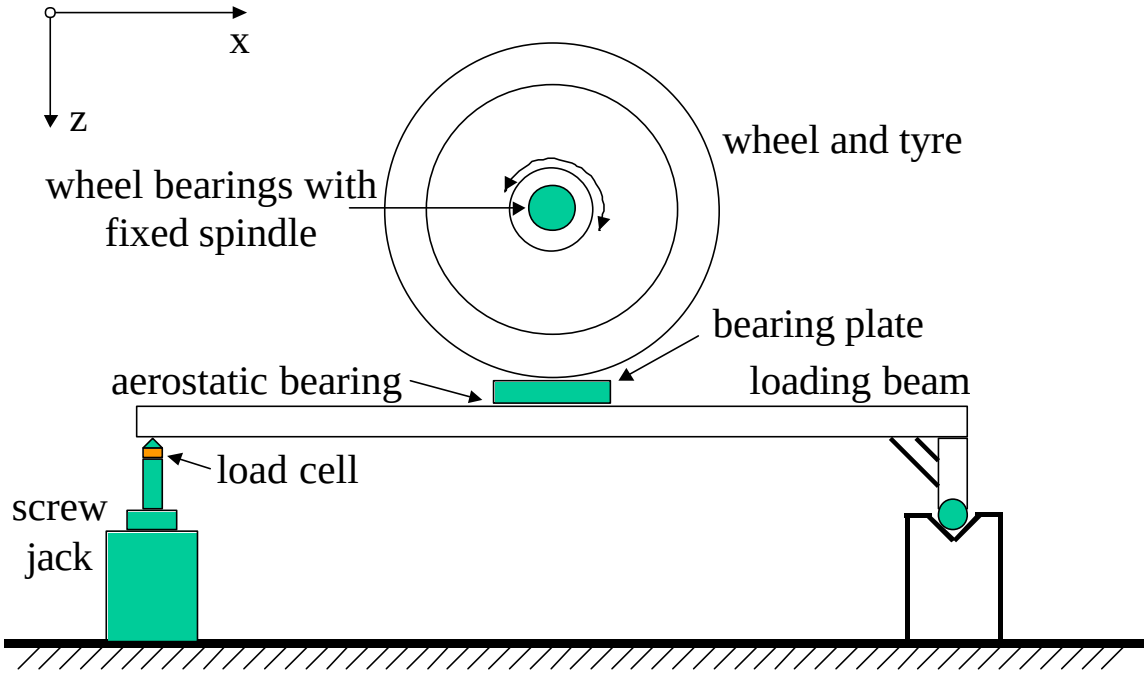

Fig. 1 Diagrammatic representation of static tyre test rig.

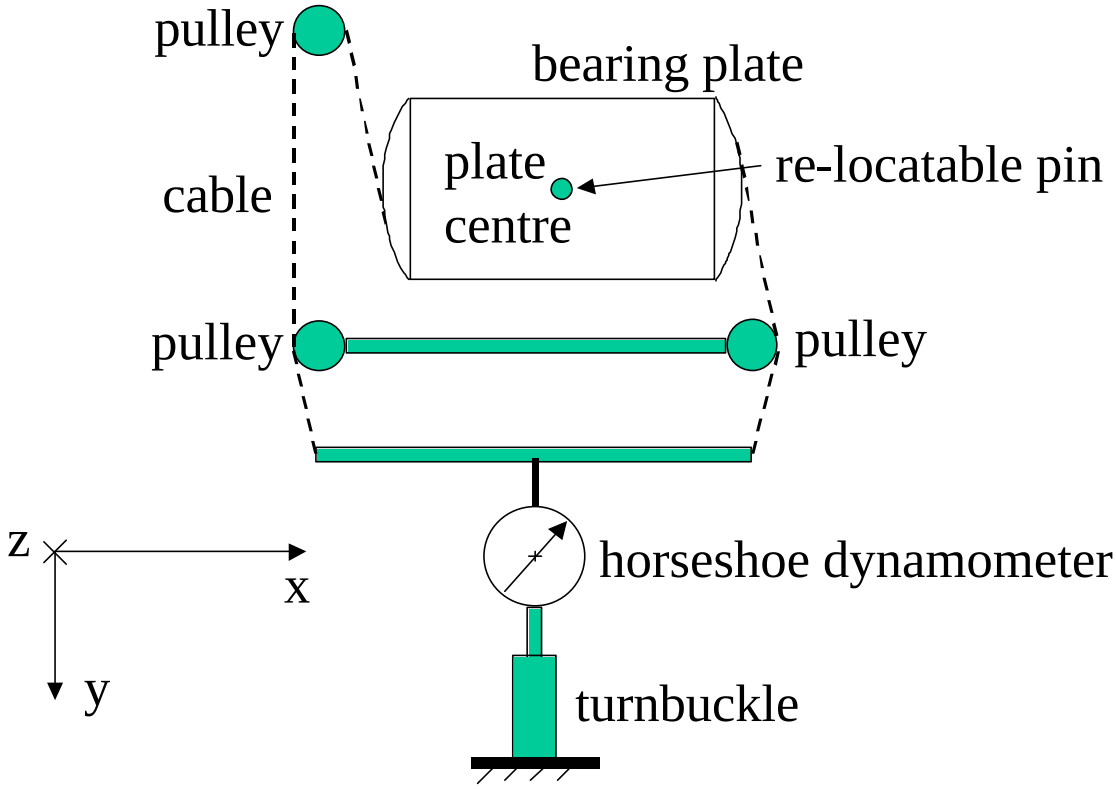

Fig. 2 Application of torque to tyre contact patch.

Initially, the applied torque acts mainly to twist the tyre sidewall structure with little sliding of the tread rubber against the plate. Later, the torque saturates at the level corresponding to sliding of the whole contact patch. This saturation torque is the one recorded for plotting. Tyre load, inflation pressure and offset were varied, with main results shown in Figs 3 and 4. The influences of load and inflation pressure variations are shown in Fig. 3. In addition, theoretical results obtained on the following basis, following Gough [1], are included. The

contact pressure between the tyre and the ground is assumed to be uniform and to be equal to the tyre inflation pressure. Also, the contact patch is treated as circular and the friction coefficient constant across the contact area. The tyre is taken to rotate around the centre of the contact area. It is easy to show that the steering torque necessary to slide the tyre over the ground is given by:

$$T = \int_0^{2p}\int_0^{R} m\, p\, r^2\, dr\, dj = \int_0^{2p} (m\, p\, R^3/3)\, dj = \frac{2p}{3} m\, p\, R^3 = \frac{2m}{3}\frac{W^{1.5}}{\sqrt{p\ p}} \qquad (1)$$

It can be anticipated that the actual torque will be a stronger function of inflation pressure than is given by equation (1), since, for low pressures, the tyre to ground contact pressure will be greater at the edges of the contact area and lesser in the middle. The converse will be true for high inflation pressures. An empirical correction to equation (1) can be applied to allow for this factor:

$$T = p_0^{(n-0.5)} \frac{2m}{3\sqrt{p}} W^{1.5} / p^n \qquad (2)$$

This form ensures that the value of T is the same as that from equation (1) at $p = p_0$ and it allows the index n to be chosen to get a better fit between experimental and theoretical results. Equation (2) is apparently able to represent the experimental rig results quite closely, if the index n is suitably chosen. Experimentation with a range of tyre types would be necessary before coming to any conclusion on how the index should change with tyre specification.

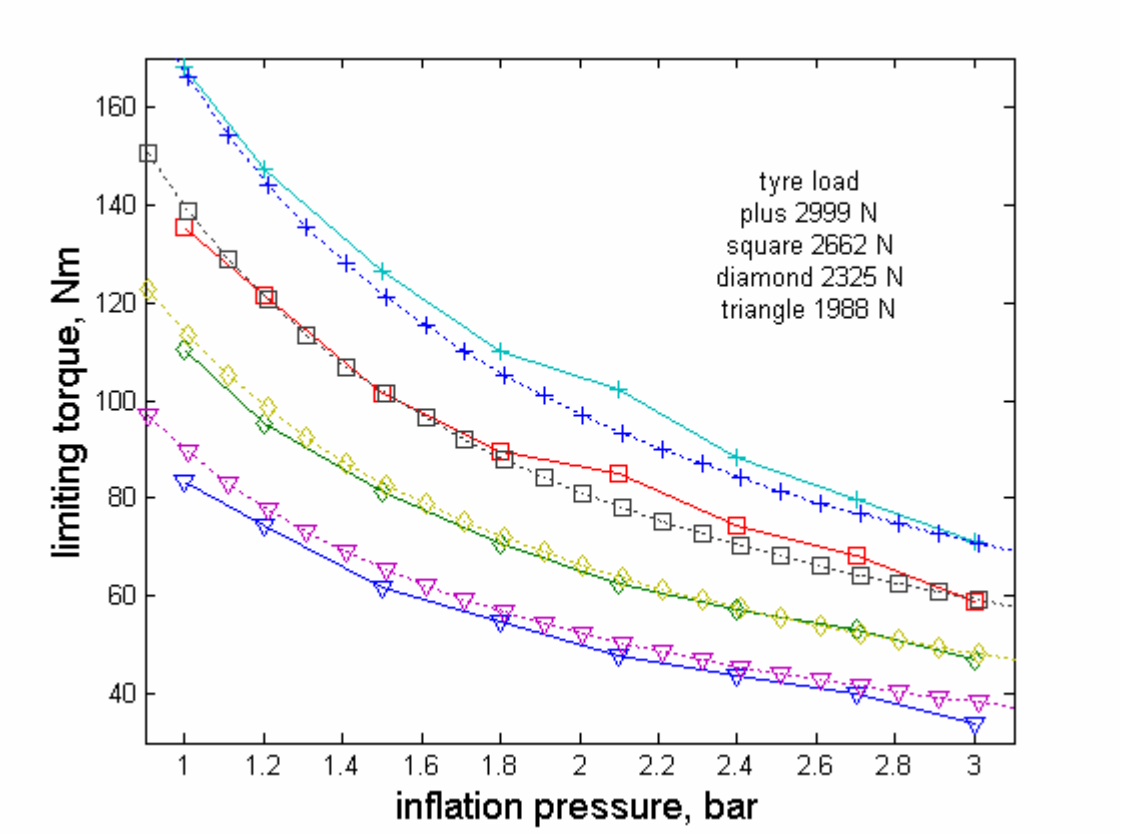

Fig. 3 Limiting torque against inflation pressure for different tyre loads. The dashed lines are theoretical results from equation (2) with $\mu = 0.666$, $p_0 = 2.45$ bar and $n = 0.78$.

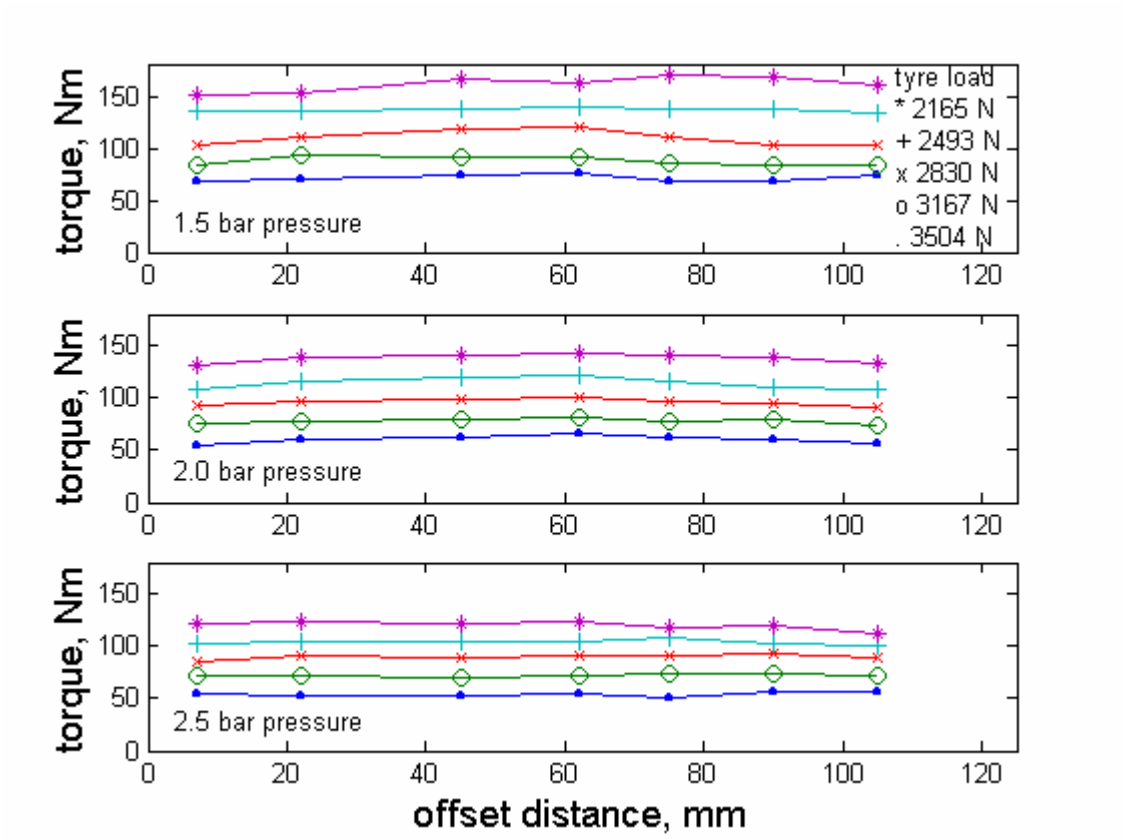

Fig. 4 Limiting torque against offset for 1.5 bar pressure; 2 bar pressure; 2.5 bar pressure and each of 5 loads.

As might be expected, the test wheel rotated in spin more, in proportion to the steer angle, as the offset increased. Detailed results are given in Table 1.

Table 1 Test wheel spin and steer angles for different offsets (263 mm tyre rolling radius).

offset, mm	steer angle, deg.	spin angle, deg.	spin/steer ratio	ratio for pure rolling	percentage difference
30	11.18	1.083	0.097	0.1141	-15.0
60	4.00	0.883	0.2209	0.2281	-3.2
105	10.18	4.08	0.4012	0.3992	+0.5

For each of the three pressures used and for all five loads, the saturation torque is substantially invariant. This is in spite of the road wheel spinning much as if its equatorial line rolled without sliding. The limiting steering torque on the rig is insensitive to the offset.

Alternatively, the wheel bearing could be locked and a longitudinal force (in the x-direction) could be applied to the loading plate, with no locating pin, until sliding of the plate relative to the tyre occurred. The ratio of shear force to normal load gives a simple measure of the tyre to loading plate friction coefficient in this test. For a load of 3660 N, a horizontal force of 2438 N was needed to slide the tyre, giving a friction coefficient of 0.666. This coefficient is used later in the system model of section 4.

3 STATIC CAR MEASUREMENTS

The car used for testing was an Austin Maestro with left hand drive. It was instrumented, so that steering wheel torque and steering rack translational displacement could be recorded.

Analogue signals were digitized via an 8-bit digital to analogue converter, part of a CIC Litecorder data acquisition system. Road wheel camber angles could be measured manually, using a Dunlop camber gauge, while the wheel loads could be determined by supporting the front tyres by Avery scales. Finer details can be found in [3]. Tests were conducted with different loads on the front wheels and offsets (by using extended wheel studs and spacers between front road wheels and hubs) and with the front tyres supported by aerostatic bearings, so that they turned freely without significant resistance from interaction with the road. Some results for different castor angles (by raising the front of the car relative to the rear) were also obtained but these are not included, due to doubts about their reliability.

In each case, the steering rack displacement is regarded as the independent variable, with the steering torque or tyre loads as dependent ones. In each test, the steering hand wheel was moved at roughly constant low speed from straight ahead to full right lock, then to full left lock and back to straight ahead again. Fig. 5 shows the steering torque as a function of rack displacement for two different loading conditions, while Fig. 6 shows the corresponding wheel load variations.

The influence of offset variation on the steering torque is demonstrated in Figs 7 and 8, the former corresponding to the tyres resting on the ground, while the latter involved the tyres being supported by the air bearings.

These experimental conditions are later used as the bases for equivalent theoretical trials, allowing comparison between the two, after the theoretical model has been set up in the next section.

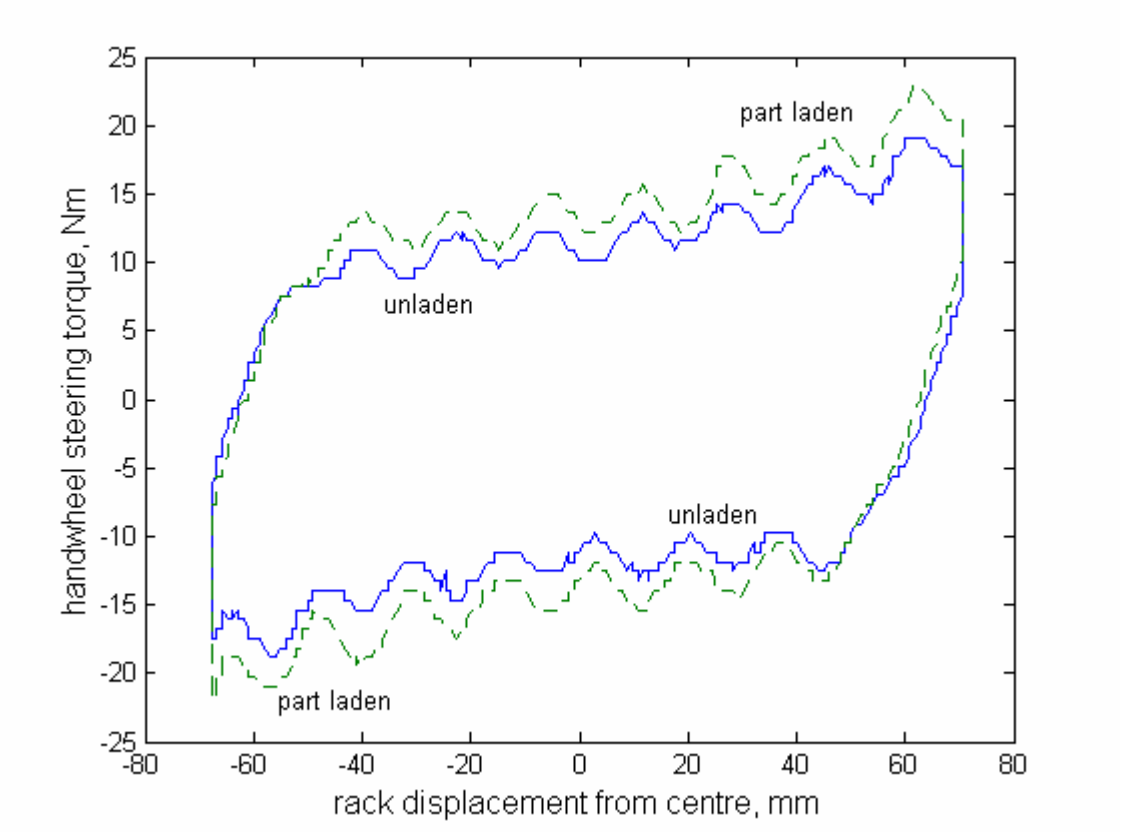

Fig. 5 Steering torque against rack displacement for unladen and part laden vehicle. The addition of the equivalent of two passengers gave a load increase of 370 N at each front wheel.

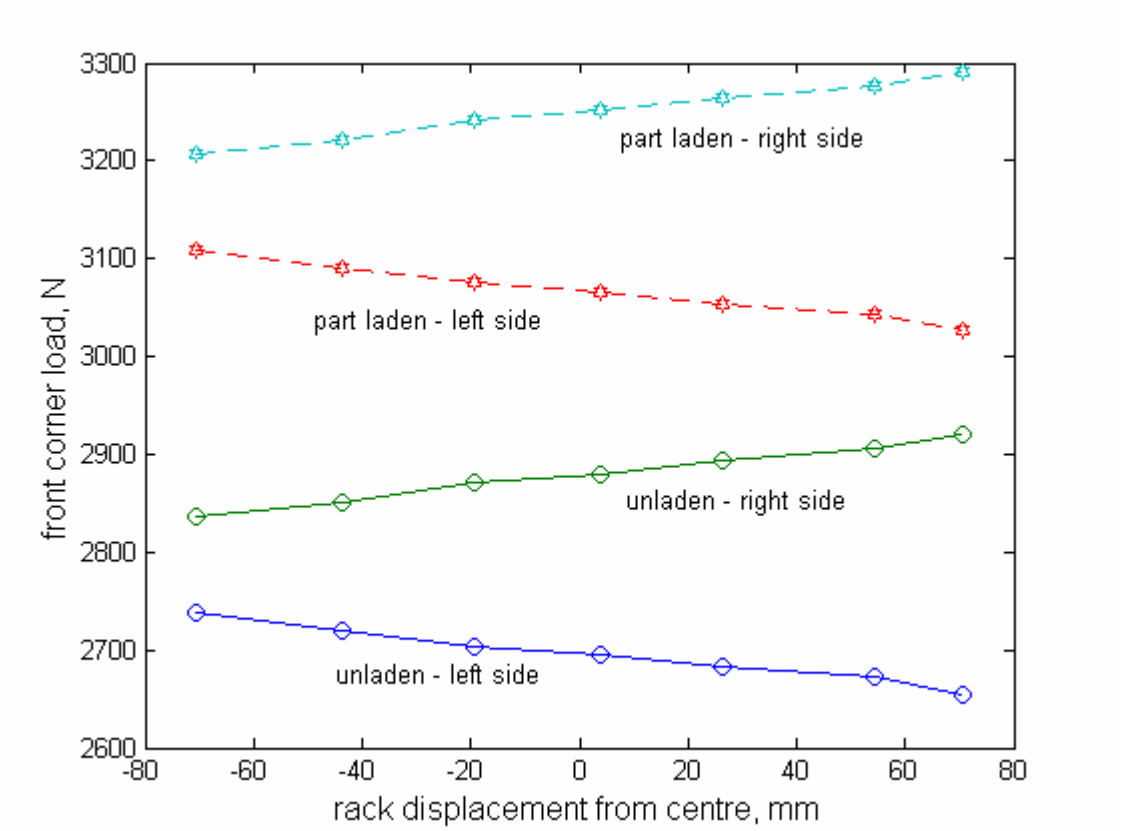

Fig. 6 Wheel loads as functions of rack displacement for unladen and part laden vehicle (conditions as Fig. 5).

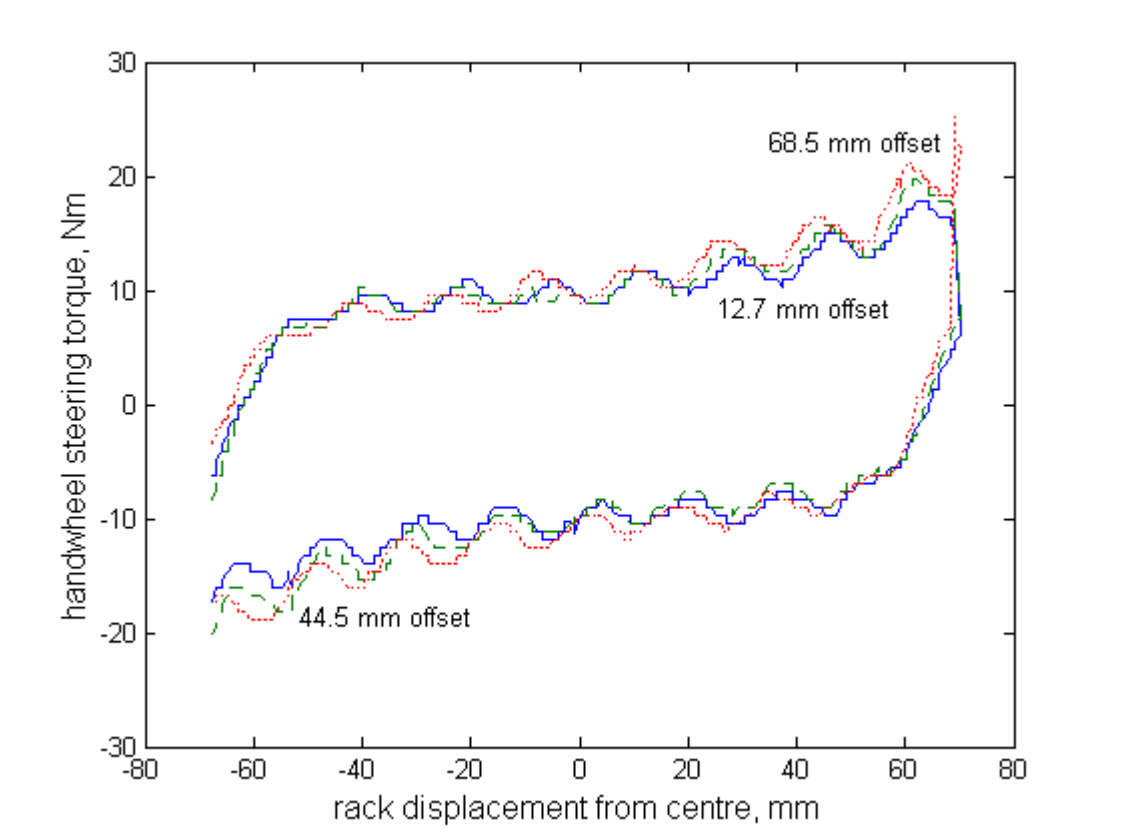

Fig. 7 Steering torque against rack displacement for each of three offsets.

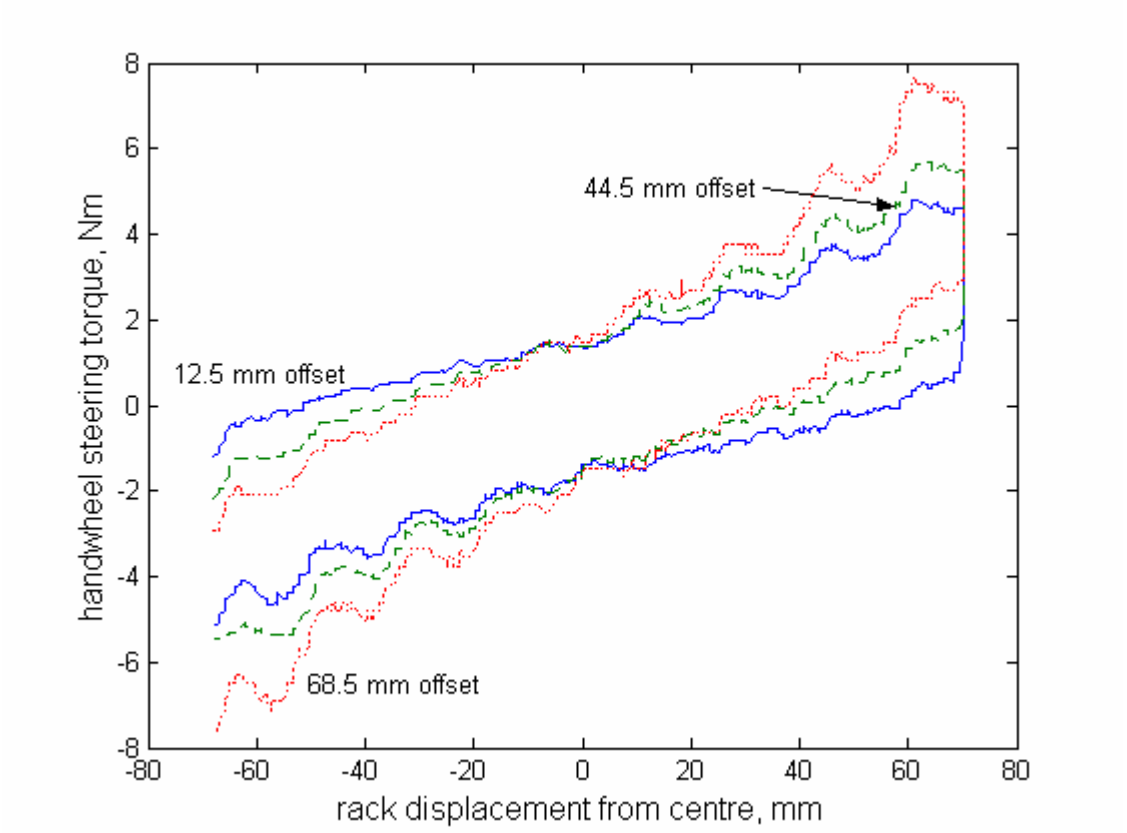

Fig. 8 Steering torque against rack displacement for each of three offsets with tyres supported on air bearings.

4 MATHEMATICAL STEERING SYSTEM MODEL AND THEORETICAL RESULTS

The mathematical model was built using AutoSim [4, http://www.trucksim.com]. AutoSim is multibody mechanical system symbolic dynamic analysis software. Its multibody language is an extension of the artificial intelligence language LISP [5]. An AutoSim program consists of text, written by way of an editor or word processor. It describes the body structure of the system, the freedoms allowed, constraints, forces and moments, inputs and outputs and a set of default parameter values. On "loading" the program into AutoSim, the symbolic equations of motion are derived using a form of Kane's equations [6, 7]. These express the principle of virtual power, so that non-holonomic constraints present no special problems. They employ generalised (minimal) coordinates, so that the bodies are normally arranged to have parent/child relationships. A "dynamics" analysis enables the writing, by AutoSim, of simulation code in the “C” language.

The hierarchical structure of an AutoSim model implies that every child inherits its parent's degrees of freedom. To these freedoms, those of the child relative to the parent are added. These relative freedoms are defined in the argument list for the child body, as can be observed below.

The car and steering system model includes only the front end of the car. The car body has bounce and roll freedoms, with roll stiffness and damping locating the body relative to the ground. Mirror image steering assemblies are fixed to the car body at right and left sides, with castor angle and king-pin inclination defining the orientations of the steering axes. In side view, the steering axis passes through the wheel centre, defining the mechanical trail through the wheel radius. In rear view, the tyre to road contact centre is offset from the

steering axis produced, Fig. 9. Rack and pinion steering is modelled, with appropriate gear ratios linking pinion to rack and rack to road wheel steer motions. The tyres are compliant vertically, with damping mainly to stabilize the simulation calculations. The tyres are also compliant in torsion, representing the flexibilities of the sidewall structures. The tread rubber is imagined attached to circumferential rings that are joined to the wheel hubs via the torsional carcass flexibilities. The torsionally compliant steering column is joined to the pinion via a Hooke's joint that operates through a significant angle, as with the car used for testing. The parent/child body structure relationships are shown in Fig. 10, with constraints shown dotted.

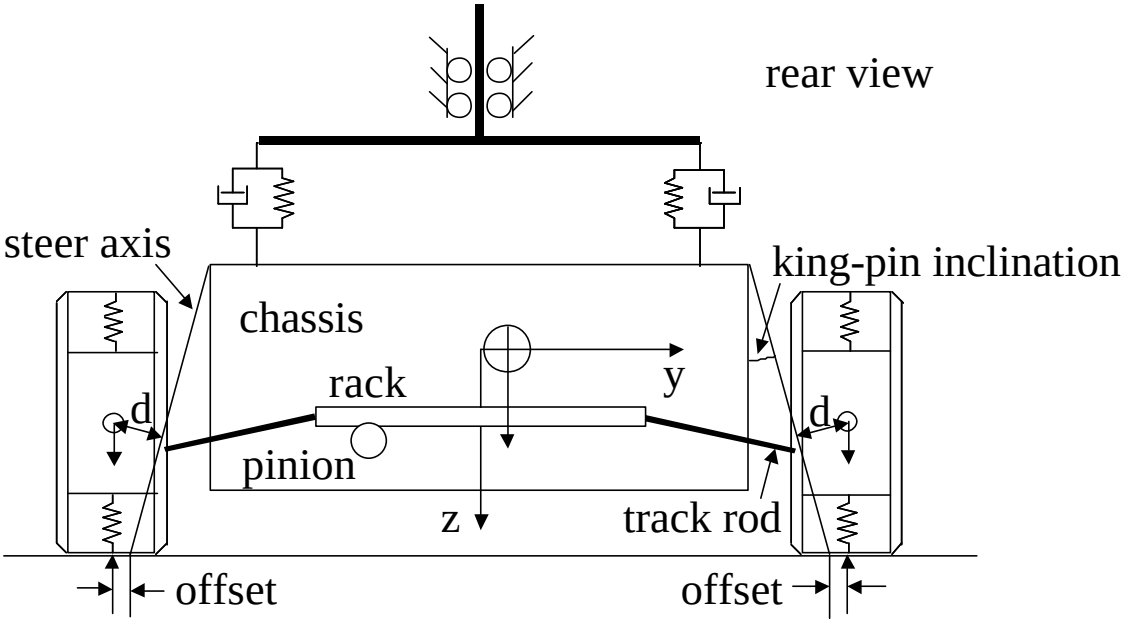

Fig. 9 Diagrammatic view of system model from rear.

The input to the system is a saw tooth steering wheel displacement, taking the steering from straight ahead to full right lock in 4.5 s, then to full left lock 9 s later, and back to straight ahead again at t = 18 s. The steering rack moves against a frictional force, made continuous in the interests of ease of integration by use of a hyperbolic tangent description, illustrated in Fig. 11. The magnitude of the force and the sharpness of the transition through zero rack speed are specified by independent parameters.

The tyre tread rubber is represented as giving a similar Coulomb friction based moment of magnitude from equation (2) with n = 0.78 and p_0 = 245000 Pa. The complete set of nominal system parameter values is given in Appendix B.

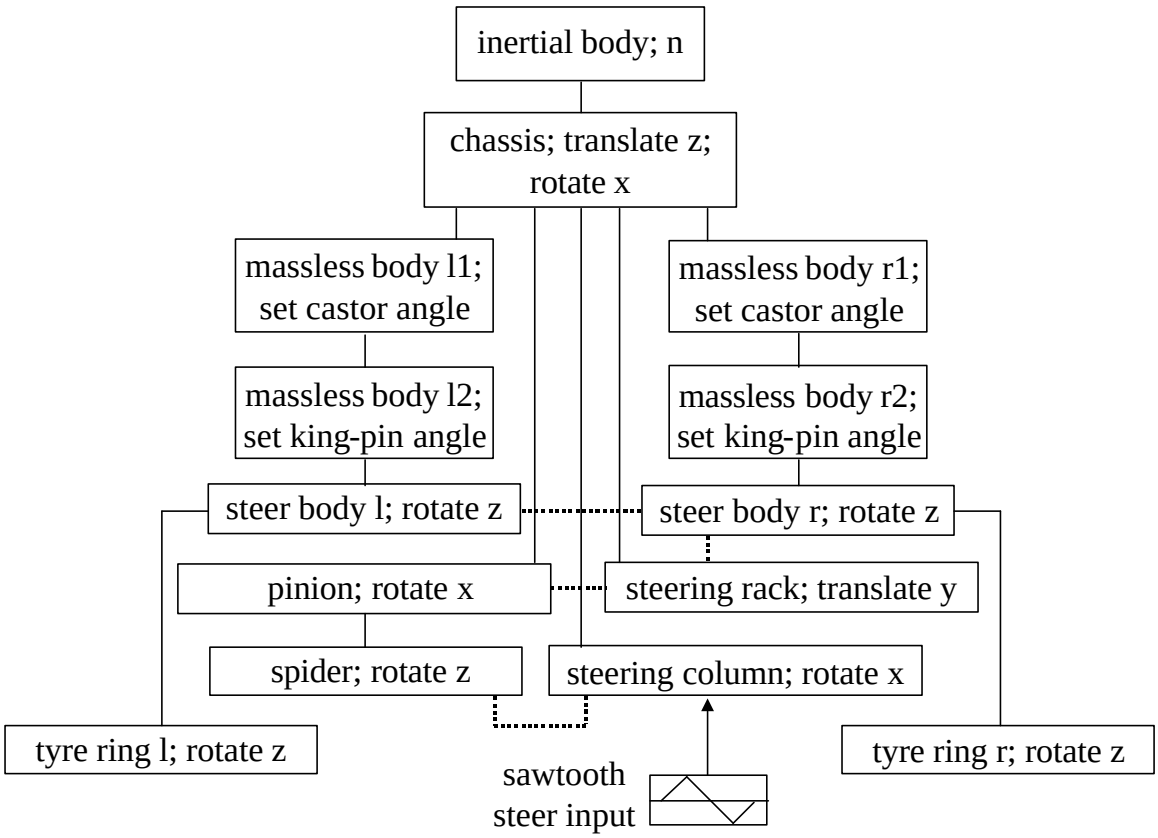

Fig. 10 Parent and child body structure relationships with constraints shown dotted.

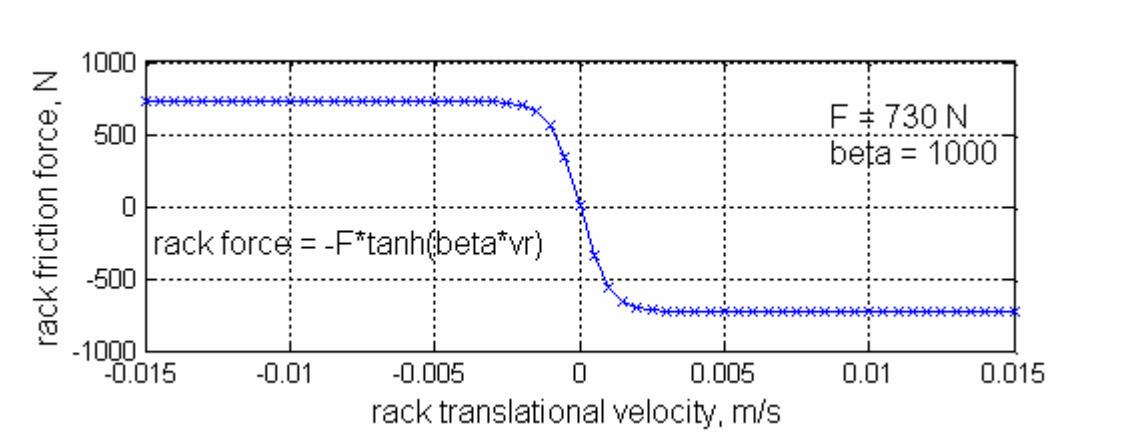

Fig. 11 Hyperbolic tangent description of steering rack friction force. A similar description is used for the tyre to ground friction moment.

The model is used first to establish the steering torque and wheel load histories of the nominal (unladen) and part laden system, in a form that can be directly compared against the measured results of Figs 5 and 6. These outputs are shown in Figs 12 and 13.

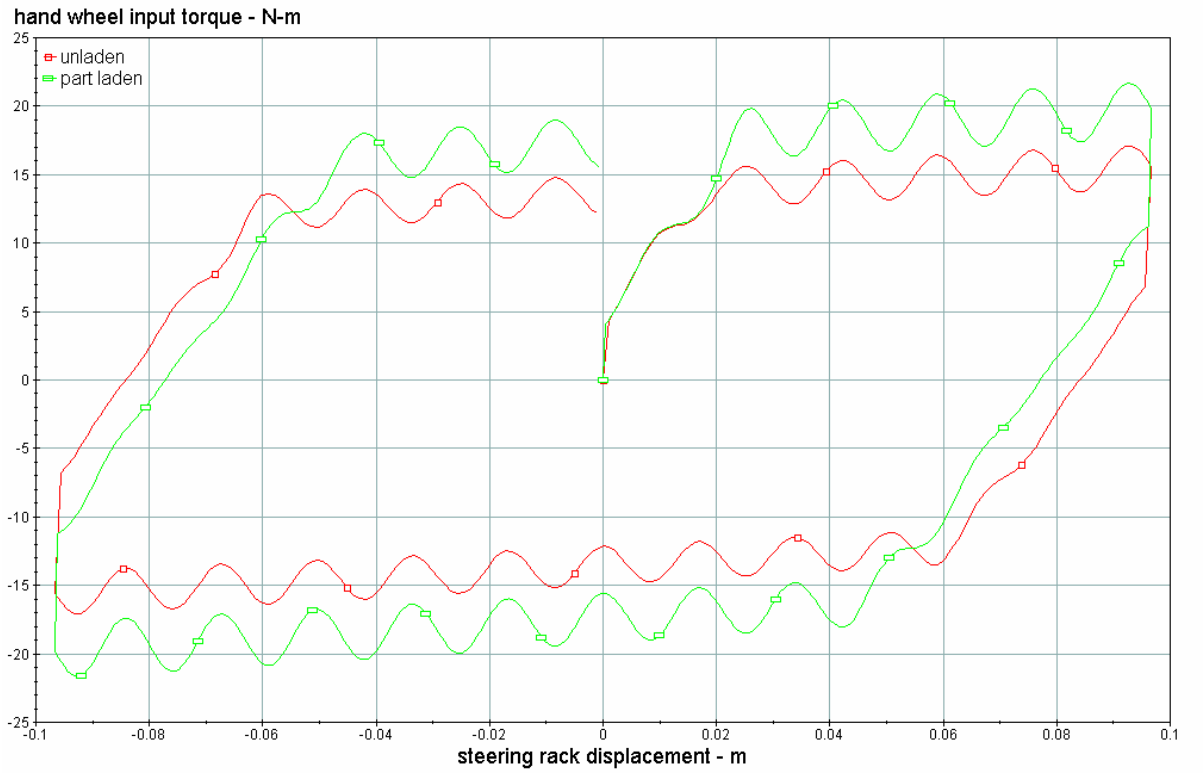

Fig. 12 Steering handwheel torque against steering rack displacement from simulation model, for nominal and part laden configurations.

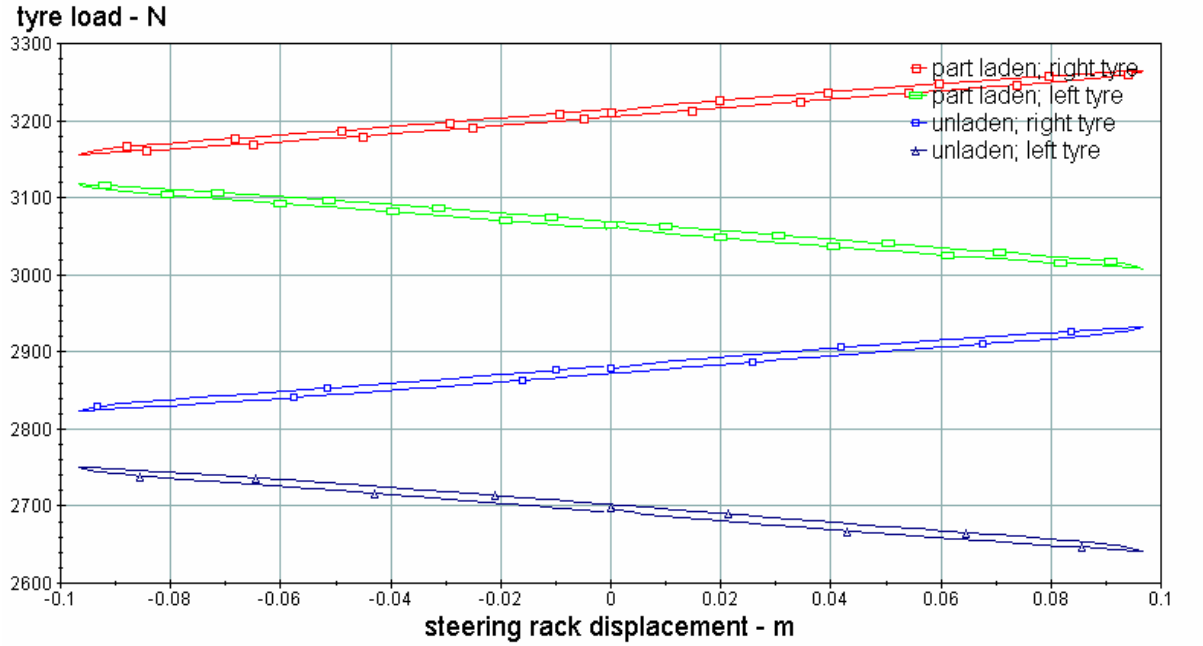

Fig. 13 Road wheel loads against steering rack displacement from simulation model, for nominal and part laden configurations.

The general form of the plots is the same as in the experiments and the quantitative agreement is good also, partly due to favourable parameter settings admittedly. The following features can be identified: From the initial, straight ahead condition, the steering has to work against rack friction and the torque rises steeply. When the torque is sufficient to move the rack, the road wheels start to steer and the tyre carcasses are twisted. The torque

rises at a rate governed by the torsional stiffness of the tyre carcass. When the tyres are sufficiently deflected, the tread rubber slides against the ground and the torque saturates at a level that reflects the load on the tyres, the tyre pressure and the friction coefficient between tyre and ground. As the steering continues, the front of the car is lifted, by virtue of the castor, king-pin inclination and offset geometry of the steering system, see Appendix A. Work is done at the steering wheel to lift the car and the steering torque has a component that depends on the rate of change of body height with steer angle. The ripple on the torque curve is caused by the non-constant velocity character of the Hooke joint in the steering column. The torque varies through two cycles for each rotation of the steering column, with an amplitude in proportion to the mean torque and governed by the joint angle.

On reversing the steering direction, the torque drops sharply corresponding to the reversal of the direction of the rack friction force, chosen in the model to give the same change in torque as in the experiments. Then the tyre carcass deformation reduces and builds up again in the reverse direction. The slope at the lower right (and upper left) of Fig. 12 depends on the tyre carcass torsional stiffness, again chosen to give the correct behaviour. The remainder of the cycle follows straightforwardly from the above description. The wheel loads have been set to agree with the measured ones for the nominal state, the right wheel being more loaded than the left one. The simulated variations with steering, Fig. 13, are similar to the actual ones, Fig. 6, with some contribution from the choice of chassis roll stiffness.

Confirmation of the influences of the individual mechanisms to the steering torque come from omitting them in turn and repeating the computations, Fig. 14 showing the results. The lifting effect is what remains if both tyre friction and rack friction are reduced to zero. In the case considered, tyre friction makes the largest contribution to the total but rack friction is substantial. The lifting effect is relatively small.

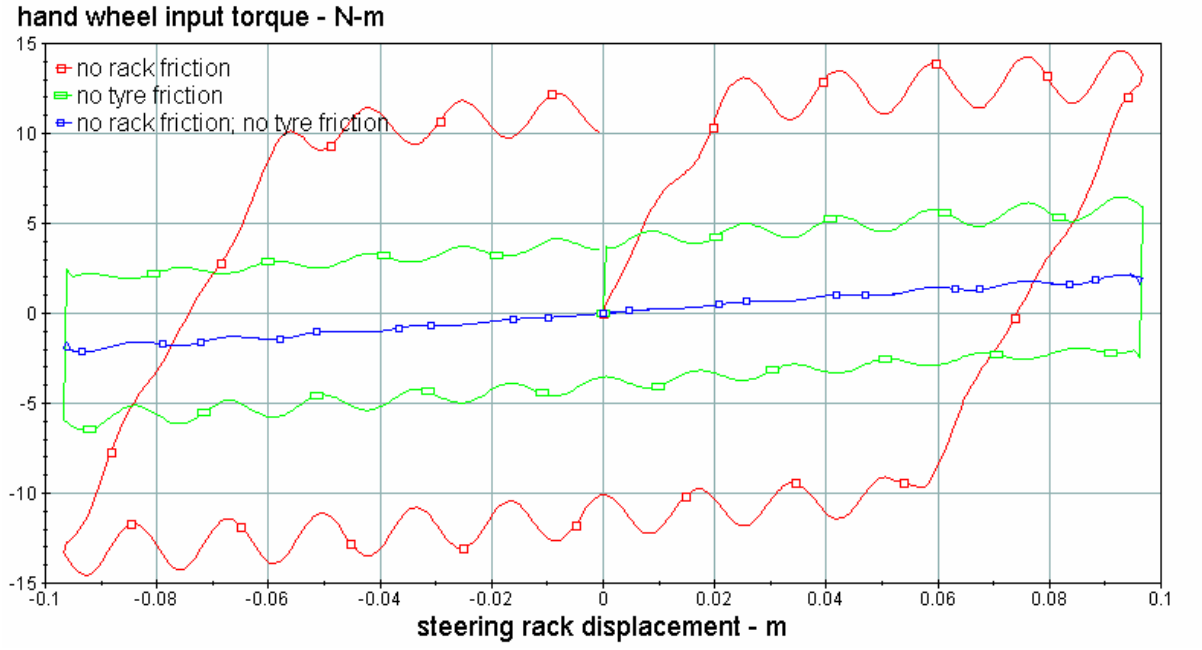

Fig. 14 Steering handwheel torque against steering rack displacement, with (a) no rack friction (b) no tyre friction (c) no rack friction and no tyre friction.

Simulation of the cycle for variations in the wheel offset yields Fig. 15, showing the very minor influence of the offset and that influence to be due to the chassis lifting effect, see Appendix A. The steering torque values are close to the experimental ones of Fig. 7. Similarly, using the model to reproduce the conditions of Fig. 8, in which the tyres were

supported on air bearings and the offset was varied, gave the results of Fig. 16, again showing a reasonable correspondence between theory and practice, although the theoretical torques are a little higher than the actual ones.

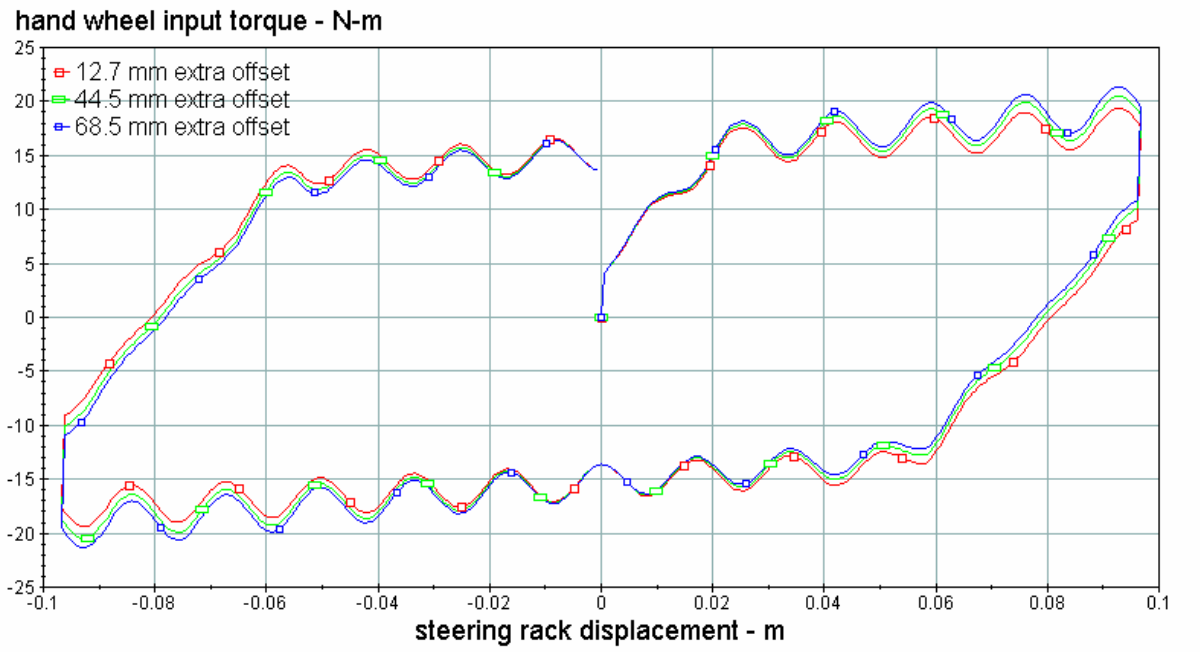

Fig. 15 Steering handwheel torque against steering rack displacement from simulation model, with variations in road wheel offset via spacers.

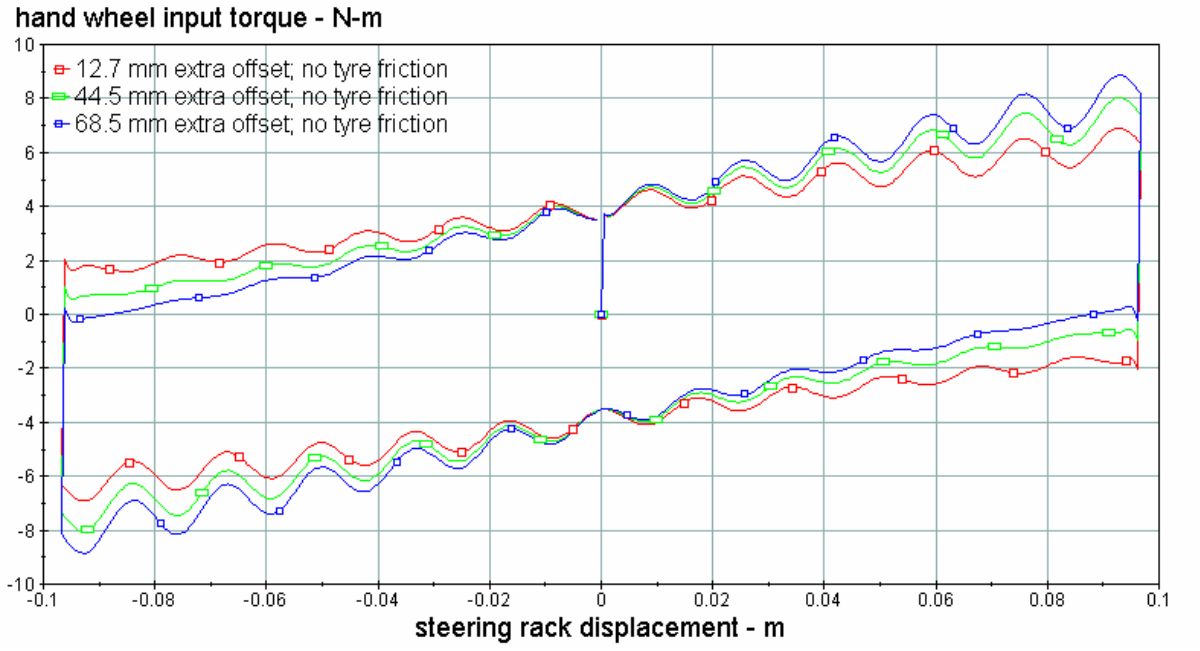

Fig. 16 Steering handwheel torque against steering rack displacement from simulation model, with no tyre friction and variations in road wheel offset.

5 INTERPRETATION OF RESULTS

The behaviour given by the system model is much the same as that of the real system. Quantitative agreement has depended on choosing some parameter values in the model to obtain a good match but the fact that this is possible supports the idea that the model is well

founded and can be used for understanding and prediction. It allows a detailed enquiry into why the steering torque behaves as it does and how to control it. The model results show how the car measurements can be interpreted in terms of the five main influences, the tyre to road friction forces, the steering mechanism friction forces, the tyre carcass flexibility, the body lifting effect and the Hooke joint angle, since each of these influences accounts for separate and identifiable parts of the steering torque cycle, as the steering moves from lock to lock. Due to the characteristic shape of the steering torque history, measurements give a direct indication of the magnitude of each influence in the system. In Appendix A, the relationship between the torque associated with lifting the chassis and the castor angle, king-pin inclination and offset distance is established and the results show that, under normal design circumstances, this contribution to the total will be a modest one. The dominant component is likely to arise from tyre to road friction interaction.

6 CONCLUSIONS

The static tyre rig results show how the torque required to steer a tyre against the effect of friction forces from the tyre to ground contact varies with load, inflation pressure and offset distance. In particular, offset has a very small influence, as suggested but not demonstrated by Gough [1]. Gough's simple analysis (equation (1)) gives a reasonable representation of the behaviour but the predictions are much better with an empirical adjustment applied to the analytical result (equation (2)).

Measurements made on the test car have been replicated quite closely by a mathematical model, having some of its parameters deriving from the car measurements. The model has allowed a detailed breakdown of all the influences in the system, such that the shape of the steering wheel torque against rack displacement graph can be interpreted in terms of the different physical effects present. Shape features are associated with sliding of the contact patch rubber across the ground, rack friction, tyre carcass twisting, lifting the car front and rotation of the Hooke joint in the steering column. Changes to each of these effects makes identifiable differences to the steering torque graph. Car measurements also confirm that steering offset has little influence on the torque requirements. Such influence as does occur is primarily due to the lifting effect that is proportional to the perpendicular distance from the wheel centre to the steer axis.

The steering torque required depends on the steering gear ratio, the total load on the front wheels, the front tyre pressures, friction in the steering system, the king-pin inclination and the castor angle. The relative importance of these features, in any particular case, is likely to be deductible from the results included in the paper.

The mathematical model, together with the adjusted analytical result and suitable other parameter values, will allow prediction of torque needs in future applications with what is expected to be adequate precision.

REFERENCES

1 **Gough, V. E.,** Discussion in London on the paper "The application of power assistance to the steering of wheeled vehicles" by F. H. Heacock and Harold Jeffrey, Proc. Aut. Div. of I. Mech. E., 1953-54, 82.

2 **Taborek, Jaroslav J.,** Mechanics of vehicles – 2, Cornering and directional control, Machine Design, June 13, 1957, 130-135.

3 Granger, R., Vehicle design and use parameters affecting the steering torque required during parking manoeuvres, Cranfield University School of Mechanical Engineering M. Sc. Thesis, August 1995.
4 Mousseau, C. W., Sayers, M. W. and Fagan, D. J., Symbolic quasi-static and dynamic analyses of complex automobile models, The Dynamics of Vehicles on Roads and on Tracks (G. Sauvage ed.), Proc. 12th IAVSD Symposium, Swets and Zeitlinger, Lisse, 1992, 446-459.
5 Steele, G. L. Jr, COMMON LISP: the language, Digital Press, Burlington, Ma, 1984.
6 Kane, T. R. and Levinson, D. A., 1985, Dynamics theory and applications, McGraw Hill, New York.
7 Riley, S. M., Model reduction of multibody systems by the removal of generalised forces of inertia, Doctoral Dissertation, University of Michigan, 2000.

Acknowledgement

Most of the work for this paper was completed while the first author was at Cranfield University School of Engineering.

Appendix A: Analysis of lifting effect from steering geometry

The left hand wheel is shown diagrammatically in Fig. A1. The points O and A are treated as fixed and the movement of the wheel centre, C, especially the vertical movement that relates to the lifting or lowering of the real car chassis when the road wheels are steered, will be

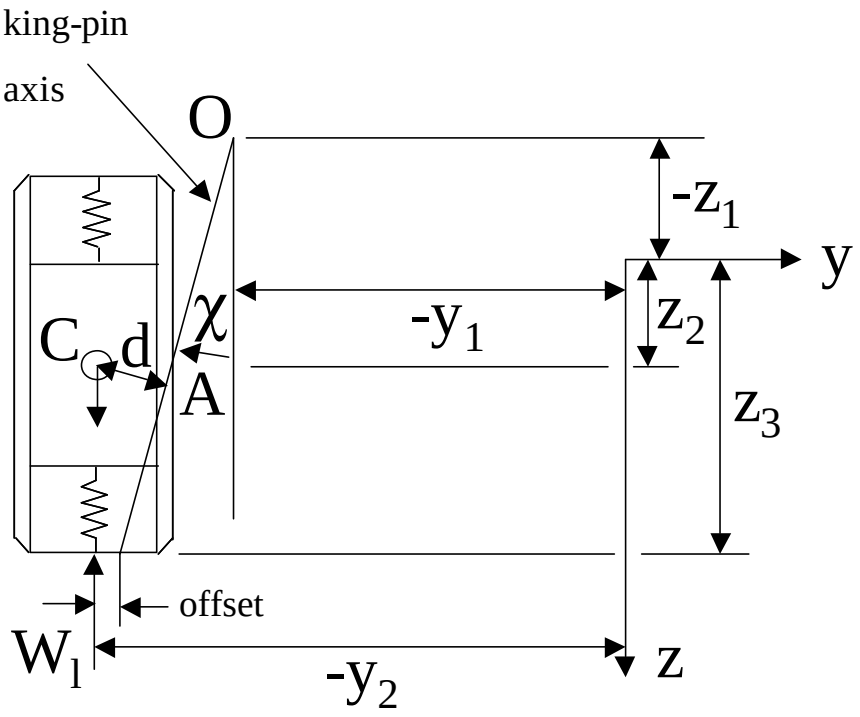

analysed.

Fig. A1 Diagrammatic representation of left front wheel, with king-pin axis and dimensions.

In Fig. A2, OX_0, Y_0, Z_0 shows the SAE standard axes. OX_0 points forwards, OY_0 points to the right, OZ_0 points vertically downwards. OA is the left wheel steering king-pin axis, while CA is the perpendicular onto the steer axis from the wheel centre. To obtain the king-

pin direction, starting from OX_0,Y_0,Z_0, the axes must rotate ε around OY_0 and then χ around OX_1. The wheel then steers by δ_w around OZ_2, C moving to C'.

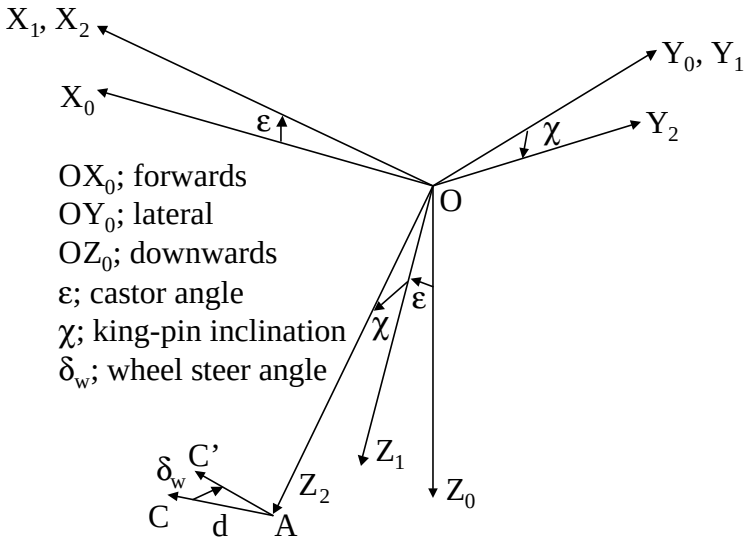

Fig. A2 Axis systems necessary to define motions of wheel centre in steering.

With O and A being fixed points, the vector AC' has components $(d.\sin\delta_w, -d.\cos\delta_w, 0)$ in the OX_2,Y_2,Z_2 system and, using standard rotational transformation matrices [6], this is $\{(d \sin\delta_w \cos\varepsilon – d \cos\delta_w \sin\chi \sin\varepsilon), (-d \cos\delta_w \cos\chi), (-d \sin\delta_w \sin\varepsilon - d \cos\delta_w \sin\chi \cos\varepsilon)\}$ in the OX_0,Y_0,Z_0 system. In particular, the vertically downward displacement of the wheel centre in a displacement δ_w from $\delta_w = 0$ is: $d \cos\varepsilon \sin\chi - d (\sin\delta_w \sin\varepsilon + \cos\delta_w \sin\chi \cos\varepsilon)$. These results have been confirmed using the symbolic capability of AutoSim. The tyre to ground contact point is, to all intents and purposes, the wheel radius below the wheel centre, so its vertical displacement is the same as that of the wheel centre. It is proportional to d, the perpendicular distance from wheel centre to king-pin axis. For the right hand wheel, the signs of d and χ are opposite and the corresponding result is $d \cos\varepsilon \sin\chi + d (\sin\delta_w \sin\varepsilon - \cos\delta_w \sin\chi \cos\varepsilon)$.

Applying the principle of virtual work to translate the lowering of the contact points against the wheel loads into steering torque, assuming a lossless mechanical connection across the system:

$$\int_0^{d_{sw}} t \, dd_{sw} = W_l\{-d \sin e \sin d + d \cos e \sin c (1-\cos d)\} + W_r\{d \sin e \sin d + d \cos e \sin c (1-\cos d)\}$$

so that:

$$t = d\{(W_r - W_l)\sin e \cos d + (W_r + W_l)\cos e \sin c \sin d\}/G \qquad (A1)$$

since $d_{sw} = Gd$

so the steering wheel torque due to lifting of the chassis by virtue of the steering geometry is proportional to the offset distance, d. The other variables combine in a sufficiently complex manner that numerical results are needed to illustrate the behaviour. Some are shown in Fig.A3 for the standard car and for each of three additional offsets. The first term on the right side of equation (A1) makes a negligible contribution, in fact, so it may be concluded that the steer torque due to lifting approximately depends on the product of the total wheel load, the cosine of the castor angle, the sine of the king-pin inclination angle and the sine of the steer angle.

In the analysis, the car body is fixed, being somewhat more constrained than in the simulation model, so the torques can be expected to be a little higher than from the

corresponding simulation. This is indeed the case, as can be observed by comparing Fig. A3 with Fig. 16.

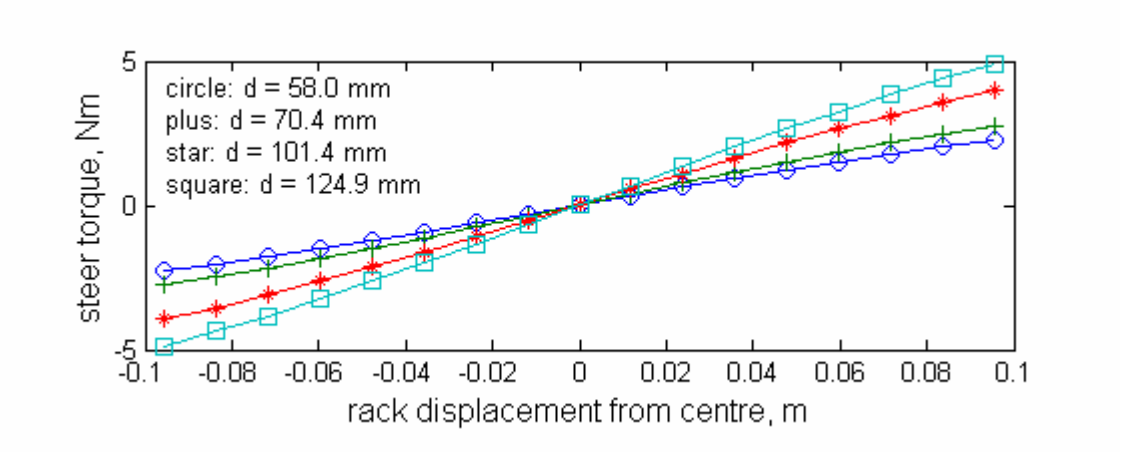

Fig. A3 Steer torque computed via equation (A1) due only to chassis lifting effects for standard car and with extra offsets 12.7, 44.5 and 68.5 mm.

Appendix B: Parameter values for simulation model (SI units)

Fixed parameters: $\beta = 1000$; steering column torsional damping coefficient = 200; tyre radial damping coefficient = 100000; chassis roll damping coefficient = 5000; tyre sidewall twist damping coefficient = 25; $\varepsilon = 0.0108$; $F = 730$; hand wheel rotation to rack translation gear ratio = 186.47; chassis roll inertia = 100; steering rack roll inertia = 0.02; yaw inertia of each tyre ring = 0.5; x-inertia of steering assembly = 1.1; y-inertia of steering assembly = 1.2; z-inertia of steering assembly = 0.8; Hooke joint angle = 0.45; steering column torsional stiffness = 1000; tyre radial stiffness = 160000; chassis roll stiffness = 300000; torsional stiffness of tyre carcass = 728; friction coefficient = 0.666; mass of steering rack = 10; mass of each tyre ring = 5; mass of each steering assembly = 40; $p = 122500$; ratio of road wheel steering displacement angle to rack translational displacement = 8.3682; mechanical trail = 0.00432; king-pin inclination angle $\chi = 0.219$; $y_1 = 0.58$; $z_1 = -0.2$; $z_2 = 0.2$; $z_3 = 0.5$.

Table B1 Variable parameters

Case:- Variable:-	Unladen (nominal)	Part laden	12.7 mm extra offset	44.5 mm extra offset	68.5 mm extra offset
Chassis mass – kg	468.4	539.76	468.4	468.4	468.4
y_{cm} – m	0.0286	0.0201	0.0286	0.0286	0.0286
y_2 – m	0.73	0.73	0.7427	0.7745	0.7985
W_l – N	2698	3065	2699.5	2703.2	2705.7
W_r – N	2878	3211	2876.5	2872.8	2870.3

The parameter values have been taken, as far as possible, from the car specification and directly from the car measurements. Otherwise they are estimates made with the intention of the simulated behaviour matching the measured behaviour. The damping coefficients are of little significance as far as the results are concerned, due to the slow pace of the motions treated, but they are important for stabilizing the solution of the equations of motion.